Theoret. Comput. Fluid Dynamics (1998) 10: 277–294

Theoretical and Computational Fluid Dynamics

Modelling Flow and Oscillations in Collapsible Tubes[1]

T.J. Pedley

Department of Applied Mathematics and Theoretical Physics, University of Cambridge,
Silver Street, Cambridge CB3 9EW, England
tjp3@damtp.cam.ac.uk

X.Y. Luo

Department of Engineering, Queen Mary and Westfield College,
Mile End Road, London EI 4NS, England

Communicated by M.Y. Hussaini

Received 19 December 1996 and accepted 16 May 1997

Abstract. Laboratory experiments designed to shed light on fluid flow through collapsible tubes, a problem with several physiological applications, invariably give rise to a wide variety of self-excited oscillations. The object of modelling is to provide scientific understanding of the complex dynamical system in question. This paper outlines some of the models that have been developed to describe the standard experiment, of flow along a finite length of elastic tube mounted at its ends on rigid tubes and contained in a chamber whose pressure can be independently varied. Lumped and one-dimensional models have been developed for the study of steady flow and its instability, and a variety of oscillation types are indeed predicted. However, such models cannot be rationally derived from the full governing equations, relying as they do on several crude, *ad hoc* assumptions such as that concerning the energy loss associated with flow separation at the time-dependent constriction during large-amplitude oscillations. A complete scientific description can be given, however, for a related two-dimensional configuration, of flow in a parallel-sided channel with a segment of one wall replaced by a membrane under longitudinal tension T. The flow and membrane displacement have been calculated successively by lubrication theory, Stokes-flow computation, steady Navier–Stokes computation and unsteady Navier–Stokes computation. For a given Reynolds number, Re, steady flow becomes unstable when T falls below a critical value (equivalently, when Re exceeds a critical value for fixed T), and the consequent oscillations reveal at least one period-doubling bifurcation as T is further reduced. The effect of wall inertia has also been investigated: it is negligible if the flowing fluid is water, but leads to an independent, high frequency flutter when it is air. The computations require very large computer resources, and a simpler model would be desirable. Investigation of the streamlines of the flow and the distribution of viscous energy dissipation reveals how the one-dimensional model might be improved; but such improvement is as yet incomplete.

[1] The work described here has been supported by the UK Engineering and Physical Science Research Council (formerly SERC) and by the Academic Development Fund of the University of Leeds, where both authors were for several years in the Department of Applied Mathematical Studies.

Foreword (by T.J.P.)

In the 1960s and 1970s Sir James Lighthill more or less single handedly transformed the application of fluid mechanics to problems in biology and medicine by a series of major research and review papers, notably on fish swimming, micro-organism swimming, and animal flight. His book, *Mathematical Biofluiddynamics*, collected this work together and added important chapters on internal or physiological fluid dynamics; the chapter on arterial pulse propagation, in particular, is a masterly exposition of the simplest and most powerful way of analysing the observed phenomena.

In 1968 I returned to England from Johns Hopkins University to work at Imperial College London with Sir James and in the new Physiological Flow Studies Unit (PFSU) which he had been instrumental in creating the year before. Soon after I arrived he showed me the results of two experimentalists at the PFSU who had observed large amplitude, self-excited oscillations while causing water to flow through an elastic tube under external pressure as a model for blood flow in an artery under an inflated blood-pressure cuff (Ur and Gordon, 1970). He suggested that I spend 6 months working out the mechanics of those oscillations. At that time I was unable to make any progress, but I have returned to the problem many times over the years, and I think we are beginning to gain some understanding.

1. Introduction

Any elastic tube will collapse if it is squeezed hard enough. If a long segment of uniform elastic tube is subjected to different levels of transmural (internal minus external) pressure, p_{tm}, the cross-sectional shape and area, A, will vary as sketched in Figure 1. When p_{tm} is large and positive, the cross-section will be circular and rather stiff because the perimeter must be stretched in order to increase A. As p_{tm} is lowered, a critical value is passed at which the circular cross-section buckles, becoming at first elliptical and then more significantly deformed. During this phase a thin-walled tube is very compliant (large area change for small pressure change) because only wall bending is required for a change of shape and hence area. At very low values of A the tube is almost totally collapsed and becomes stiff again. During the compliant phase, even the small pressure changes associated with flow through the tube (viscous or inertial) can be enough to cause collapse.

The collapse of compressed elastic tubes conveying a flow occurs naturally in several physiological

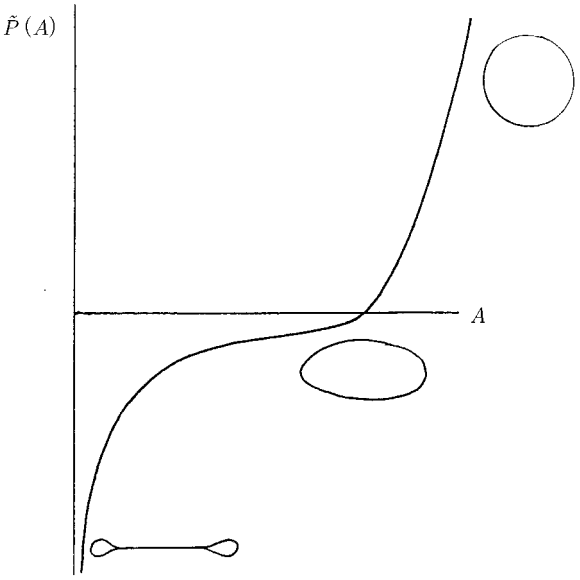

Figure 1. Sketch of the "tube law" for a collapsible tube, relating transmural pressure $\tilde{P}$ and cross-sectional area A. Sketches of the cross-sectional shape are given for three regions of the curve.

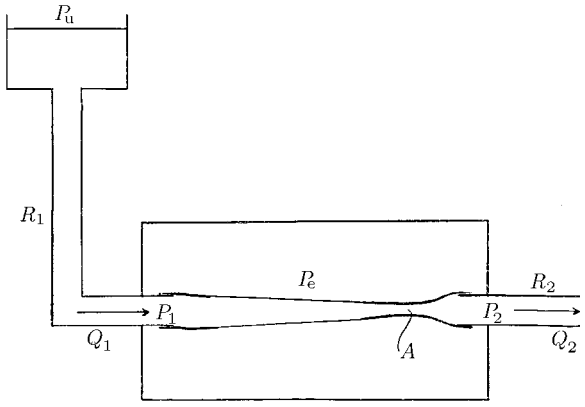

Figure 2. Sketch of the standard laboratory experiment. P_1, Q_1 are pressure and flow rate upstream of the collapsible segment; P_2, Q_2 are pressure and flow rate downstream; P_u is total pressure far upsteam; P_e is pressure in the chamber surrounding the collapsible segment. R_1 and R_2 represent the rigid pipes up- and downstream, whose resistance can be prescribed.

applications. Examples include: (i) Blood flow in veins, either above the level of the heart where the internal pressure may be subatmospheric because of the effect of gravity (the jugular vein of the giraffe is particularly interesting in this context (Pedley *et al.*, 1996)), or being squeezed by contracting skeletal muscle as in the "muscle pump" used to return blood to the heart from the feet of an upright mammal. (ii) Blood flow in arteries, such as intramyocardial coronary arteries during the contraction of the left ventricle, or actively squeezed by an external agency such as a blood-pressure cuff. (iii) Air flow in the large intrathoracic airways of the lung during a forced expiration or cough, because an increase in alveolar air pressure, intended to increase the expiratory flow rate, is also exerted on the outside of the airways. In this case, increasing alveolar pressure above a certain level does not increase the expiratory flow rate, a process known as *flow limitation*. (iv) Urine flow in the urethra during micturition, where flow limitation is again commonplace. These and other examples are discussed in greater detail by Shapiro (1977a,b). Note that in all the cases mentioned the Reynolds number of the flow (Re) is in the hundreds or higher.

Many workers have performed laboratory experiments on nominally steady flow through collapsible tubes. In the standard experiment a segment of collapsible (e.g., rubber) tube is mounted at its ends on rigid tubes and contained in a chamber whose pressure, p_e, can be independently controlled; the behaviour of the system depends on two independent pressure *differences*, e.g., $p_u - p_d$ and $p_e - p_d$. Some early experimental studies sought to characterize the collapsible tube by plotting the pressure difference along it ($\Delta p = p_1 - p_2$: see Figure 2) against the flow-rate, q; there was some confusion in the literature because it was not always clear which controlled pressure difference was being varied, as flow rate was varied, and which was held constant. Three different examples, in each of which the shape of the $\Delta p - q$ curve is quite different, are shown in Figure 3(a,b,c), taken from Brecher (1952), Bertram (1986), and Conrad (1969), respectively. For explanation of the different curves see Kamm and Pedley (1989).

In almost all such collapsible tube experiments with $Re \gtrsim 200$, ranges of parameters were found in which steady flow could not be achieved but, instead, large-amplitude, flow-induced oscillations were observed. Bertram and his colleagues (1982, 1986, 1990, 1991) have made probably the most systematic series of experiments on self-excited oscillations in collapsible tubes, recording as functions of time the pressures (p_1, p_2) and flow rates (q_1, q_2) at the upstream and downstream ends of the collapsible segment, and the cross-sectional area A_n at the narrowest point. Examples of some of the measurements of $p_2(t)$ for various parameter values are shown in Figure 4; a great variety of oscillatory behaviour is exhibited. Bertram *et al.* (1990) have tried to map out the associated control space diagrams, to identify regions in which different types of oscillation arise. All that can be said in summary is that a finite length of compressed collapsible tube conveying a flow represents a dynamical system of remarkable richness and complexity. It would clearly be of great interest to be able to model the system theoretically and hence understand it physically. That interest is independent of any relevance, though it should be noted that flow-induced oscillations do arise in some of the physiological applications: wheezing during forced expiration; the Korotkov sounds listened for during blood pressure measurement with a cuff; and "cervical venous hum" (Danaky and Ronan, 1974) are but three examples.

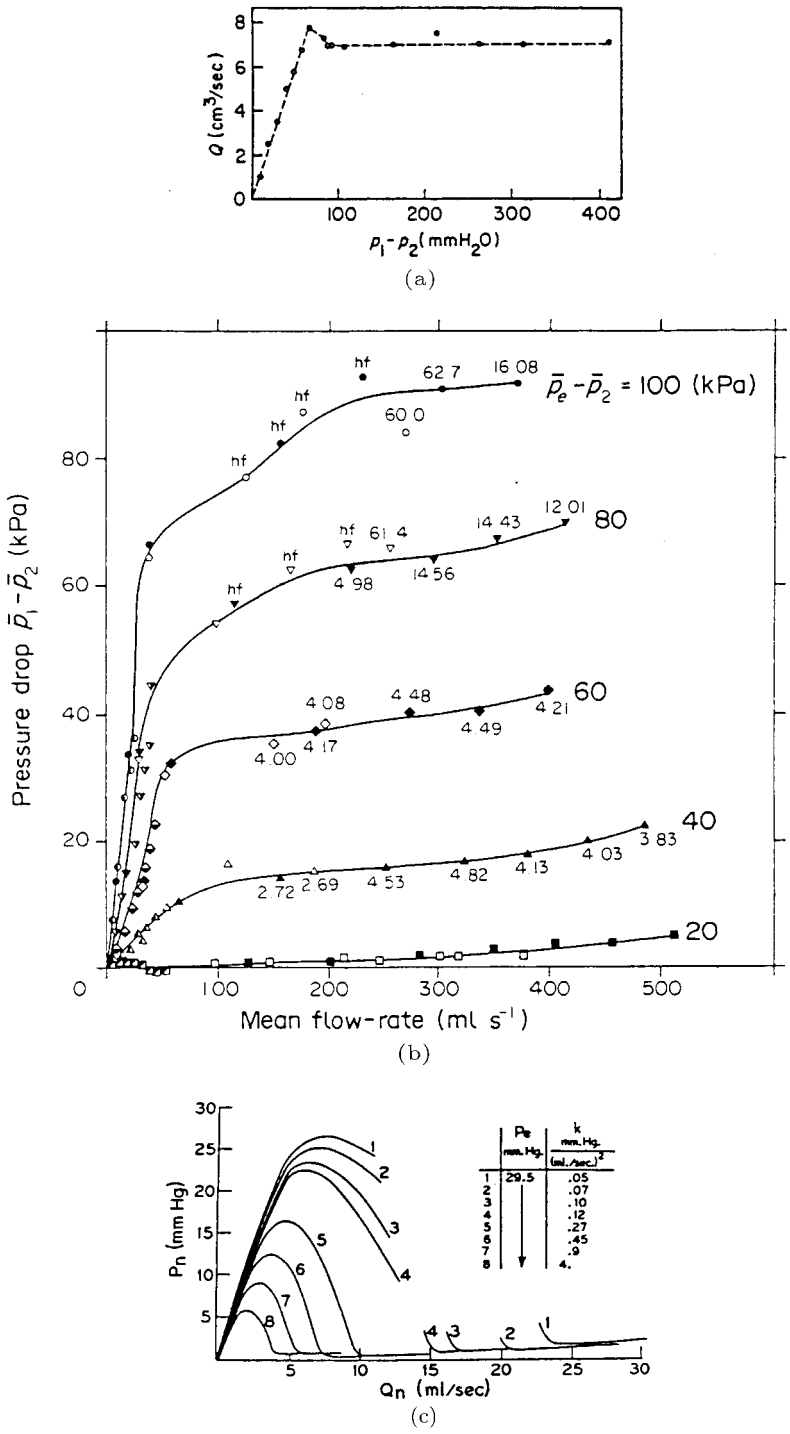

Figure 3. Pressure drop $p_1 - p_2$ along the collapsible segment, plotted against flow-rate q for three different conditions: (a) $p_u - p_e$ held constant (from Brecher, 1952); (b) $p_e - p_2$ held constant (from Bertram, 1986); (c) $p_e - p_d$ held constant (from Conrad, 1969).

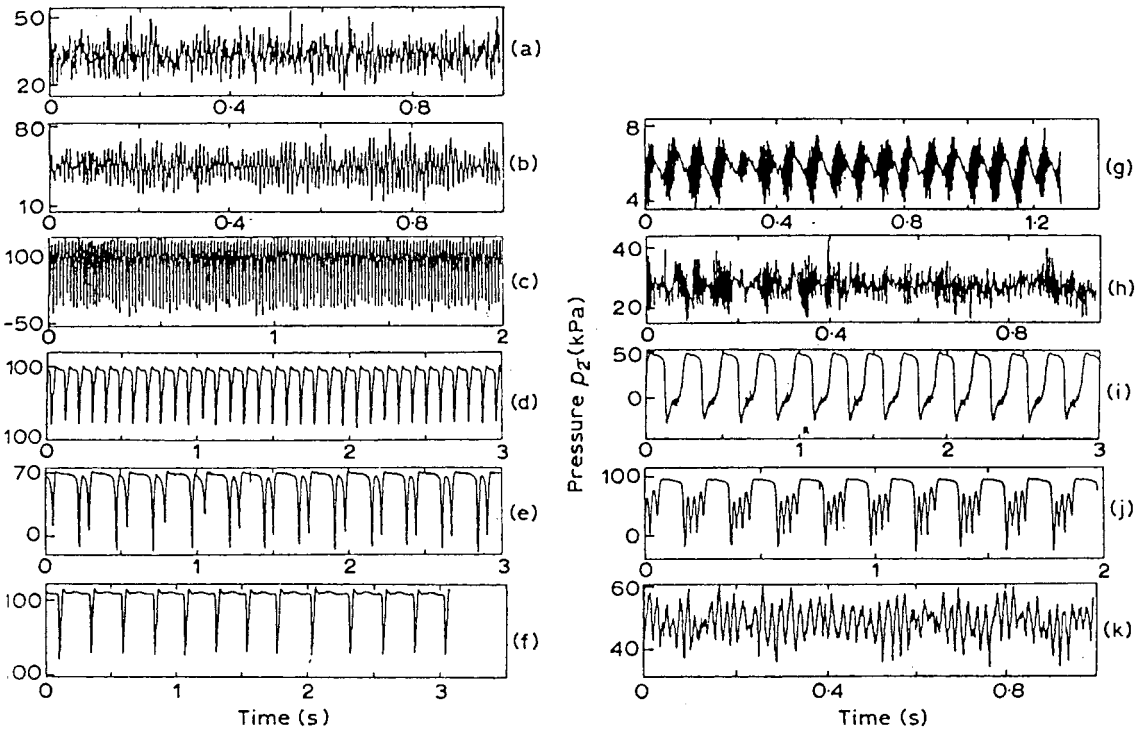

Figure 4. Pressure, p_2, at the downstream end of the collapsible segment, plotted against time t during self-excited oscillations for various values of the governing parameters (from Bertram *et al.*, 1991).

2. Zero- and One-Dimensional Models

The earliest and simplest theoretical models of collapsible-tube flow were lumped-parameter or zero-dimensional models, in which the relevant variables were functions only of time t, and satisfied non-linear ordinary differential equations. The geometry of the whole collapsible segment would be represented, say, by the cross-sectional area at the narrowest point, $A_{\rm n}(t)$, and the other variables would be the pressure at that point, $p_{\rm n}(t)$, together with the measurable quantities $p_1(t), p_2(t), q_1(t), q_2(t)$. The variables were linked by dynamical equations representing conservation of mass and momentum, together with a *tube law* (Figure 1) relating the transmural pressure $p_{\rm n} - p_{\rm e}$ and the area $A_{\rm n}$, but only at the narrowest point. The system of ordinary differential equations was typically of second or third order (Conrad, 1969; Schoendorfer and Shapiro, 1977; Pedley, 1980, Chapter 6; Bertram and Pedley, 1983), though the well-known model of Katz *et al.* (1969) was of fifth order. Some authors, in the days before modern dynamical systems theory, were content to imply that, since both their experiments and their model produced oscillations, the problem was solved. Because many real mechanical features cannot be incorporated in lumped-parameter models, we do not discuss them further here.

The next level of sophistication is a one-dimensional model, in which the pressure p and the longitudinal velocity u, both averaged across the tube cross-section, together with the cross-sectional area A, are regarded as functions of the longitudinal co-ordinate x and time t. For steady flow, without t-dependence, the governing equations have traditionally been taken to be the following (Shapiro, 1977a):

$$\text{conservation of mass} \qquad \frac{d}{dx}(uA) = 0, \tag{1}$$

$$\text{conservation of momentum} \qquad u\frac{du}{dx} = -\frac{1}{\rho}\frac{dp}{dx} - R(A,u)u, \tag{2}$$

$$\text{elasticity (tube law)} \qquad p - p_{\rm e} = \tilde{P}(A), \tag{3}$$

where the function $\tilde{P}(A)$ represents the tube law (Figure 1). In (2) the body-force term has been omitted since the longitudinal component of gravity is equivalent to a gradient in external pressure, $p_{\rm e}$. The convective

inertia term does not include the contribution from the non-flat velocity profile, which can in general be incorporated into the term, Ru, representing viscous resistance; R is assumed to be positive. The set of equations (1)–(3) are exactly analogous to those for water flow in shallow channels with a free surface.

Henceforth we take p_e to be constant. Eliminating p from (2) and (3) we find the rate of change of A with distance to be

$$\frac{dA}{dx} = \frac{-RuA}{c^2 - u^2}, \tag{4}$$

where

$$c^2 = \frac{A}{\rho}\frac{d\tilde{P}}{dA}. \tag{5}$$

It can readily be shown that c is the speed of propagation of long, small-amplitude pressure (or area) waves along the tube when its cross-sectional area is A (Lighthill, 1975). Suppose that, at an upstream station, the tube is circular and $u < c$. Then (4) shows that dA/dx is negative. Now the flow rate $uA = q$ is constant so, as A decreases, u increases; moreover the slope of the tube law, and hence c, will if anything decrease, so $c^2 - u^2$ becomes smaller. Hence dA/dx becomes more negative. If the tube is long enough, a point will in general be reached at which u is predicted to be equal to c so $dA/dx = -\infty$. By this stage, referred to as *choking*, the steady flow model will clearly have broken down: steady flow at the proposed flow rate q, from the postulated upstream conditions, is not possible. If q and the upstream area are held fixed, and the model is a correct one for steady flow, then unsteady behaviour must follow. A number of authors (e.g., Brower and Scholten, 1975) have gone further and suggested that the presence of a point at which the fluid speed is equal to the wave speed is the prime mechanism for the initiation of unsteady behaviour—i.e., of self-excited oscillations.

However, the one-dimensional model contained in (1)–(3) must break down anyway, even without choking, in order to describe the experiment depicted in Figure 2, because dA/dx would have to become positive again near the downstream end $x = l$. Cancelli and Pedley (1985) added two new features, both of which should be important in the region downstream of the narrowest point. One was longitudinal tension in the tube wall, the simplest model for which causes (3) to be replaced by

$$p - p_e = \tilde{P}(A) - T\frac{d^2A}{dx^2}. \tag{6}$$

In the highly collapsed region the tube wall resembles two flattish membranes under tension, with longitudinal curvature roughly proportional to d^2A/dx^2. It was felt that the addition of extra x-derivatives would enable more boundary conditions to be applied, such as $A(\ell) = A(0) = A_0$. The other new feature was the recognition that flow through a constriction will separate, a process leading to enhanced energy loss and therefore substantially incomplete pressure recovery in the region downstream of the narrowest point . The energy loss downstream of the narrowest point had already been identified as important in lumped-parameter models (Pedley, 1980). Cancelli and Pedley (1985) used momentum arguments to suggest that a reasonable, yet still simple, model of the energy loss could be achieved by replacing equation (2), downstream of the narrowest point, by

$$\chi u\frac{du}{dx} = -\frac{1}{\rho}\frac{dp}{dx}, \tag{7}$$

where χ is a non-negative quantity, less than 1; in their (unsteady) calculations Cancelli and Pedley took $\chi = 0.2$.

The steady flow model described by (1), (6) and (7) with

$$\begin{aligned} \tilde{P}(A) &= K_p(1 - \alpha^{-3/2}) \qquad \text{for} \quad \alpha < 1 \\ &= K_p k(\alpha - 1) \qquad \text{for} \quad \alpha > 1 \end{aligned} \tag{8}$$

(where $\alpha = A/A_0$, K_p is a constant, and the $-3/2$ power in the last term comes from a similarity solution derived for small α by Flaherty *et al.* (1972)), was exhaustively analysed by Jensen and Pedley (1989). These authors neglected the direct viscous term Ru, taking $\chi = 1$ for $0 < x < x_s$ (the unknown point of flow separation, taken to be identical with the narrowest point at sufficiently high Reynolds number) and

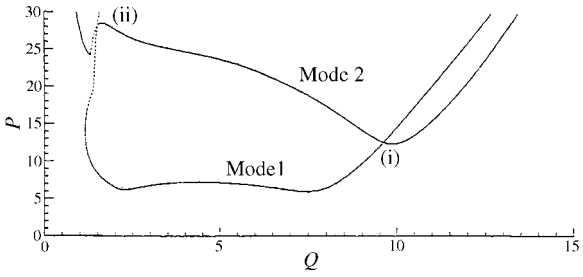

Figure 5. Stability boundaries for the first two modes of instability, plotted on the dimensionless P–Q plane ($P \propto p_e - p_2$; $Q \propto q$), as predicted by the one-dimensional model of Jensen (1990). The Hopf bifurcations are subcritical where the curves are dotted, supercritical elsewhere; (i) and (ii) are mode crossing points.

χ = constant ≤ 1 for $x_s < x < l$. Their principal results can be summarized as follows:

(i) When $\chi = 1$ everywhere, i.e., there is no energy loss in the collapsible tube downstream of the narrowest point, then there exists a critical value of the flow rate q, dependent on the longitudinal tension T, above which the steady problem has no solution. In other words, the presence of longitudinal tension alone does not abolish choking; this should not have been a surprise: in the same way, surface tension does not abolish critical behaviour in shallow-water channel flow.

(ii) However, whenever there is any downstream energy loss, i.e., $\chi < 1$ for $x_s < x < l$, then a steady solution exists for all positive values of flow rate q and tension T. Since some such energy loss in inevitable, it follows that the breakdown of steady flow is not caused by choking, i.e., the non-existence of a steady flow at the chosen parameter values, but must arise through instability of the steady solution.

Jensen (1990) gave a detailed linear, and weakly non-linear, analysis of the instability of the steady flow. He used the same one-dimensional model with the addition of time derivatives, $\partial A/\partial t$ and $\partial u/\partial t$, on the left hand sides of (1) and (7) respectively. The elasticity equations (6) and (8) remained unchanged. When appropriately non-dimensionalized, Jensen's model has two principal governing dimensionless parameters, in addition to χ (which was fixed at a value of 0.2 in all numerical computations): Q, which is proportional to the flow rate q, and P, proportional to the transmural pressure, $p_e - p_2$, at the downstream end of the collapsible segment when the flow is steady. Other parameters describe the resistance and inertance of the upstream and downstream rigid segments; these were kept fixed throughout. Figure 5 shows the computed stability boundaries in the P–Q plane, for the first two instability modes found. The general shape, showing stable steady flow for sufficiently small P at all Q (the tube remaining effectively open), and for sufficiently small Q at all P (the tube being collapsed when P is large enough), is in qualitative agreement with the control diagrams plotted by Bertram *et al.* (1990). So too are the presence of mode crossing points (i) and (ii) and the existence of several regions in parameter space in which different behaviour of the system is to be expected. Jensen's weakly non-linear analysis showed that both modes become unstable through supercritical Hopf bifurcations everywhere except for the small segments of the stability boundaries marked as dotted in Figure 5, where they are subcritical Hopf bifurcations.

In a subsequent paper Jensen (1992) showed some results of a numerical integration of the fully non-linear one-dimensional equations, at a few selected points in parameter space, near the upper left mode crossing point in Figure 5. Some of the computed time series, of $p_2(t) = p(l, t)$ for example, look quite similar to the measurements of Bertram *et al.* (1990). It is clear that this one-dimensional model contains much that is relevant to the self-excited oscillations of real collapsible tubes in the laboratory. It would be possible to extend Jensen's (1992) full non-linear computations to cover the whole of parameter space, and map out the behaviour in as much (or more) detail as has been done experimentally.

However, this has not been done, and should not, because of the severe *a priori* weaknesses of the one-dimensional model as a scientific description of the real system. First, the solid mechanics of (6) and (8) is an extremely crude representation of the non-axisymmetric, large deformation of a cylindrical shell under prestretch, external pressure, and the stresses exerted by internal flow. Second, the fluid mechanics is also extremely crude, primarily because of the *ad hoc* way of representing flow separation and the processes of energy loss/pressure recovery downstream of the constriction. This is especially weak in unsteady flow, since the arguments leading to (7) were based on steady flow (Cancelli and Pedley, 1985) and take no account, for example, of the time delay between the emergence of a sufficiently adverse pressure gradient and the breakaway of previously attached flow (see the experiments of Bertram and Pedley (1983)). What is

required is a solution of the unsteady, three-dimensional Navier-Stokes equations, coupled to the equations for the unsteady, three-dimensional, large-deformation theory of highly compliant shells. Numerical codes for the solution of such problems are not yet available in any branch of computational mechanics, and would require resources in excess of any available to us. The nearest we have been able to approach is to solve the full shell-deformation problem with steady viscous flow in the tube described by lubrication theory (Heil and Pedley, 1996) so that oscillations cannot arise.

3. Two-Dimensional Models

Instead of attempting the full three-dimensional problem, we have sought a sound scientific solution for a simpler, two-dimensional configuration which is nevertheless in principle realizable experimentally. The configuration is sketched in Figure 6. A two-dimensional channel consists of two parallel, rigid planes, distance h_0 apart, from one of which a segment of length Lh_0 has been removed and replaced by a thin membrane, with no bending stiffness or inertia but under longitudinal tension T. Steady, plane Poiseuille flow with flow rate q enters far upstream. The external pressure takes a constant value, p_e, referred to the pressure at the far end of the downstream rigid segment.

In all the following discussion, lengths are made dimensionless with respect to h_0, and the position of the membrane is given by

$$y = h(x,t), \qquad 0 \le x \le L, \tag{9}$$

where $h(0,t) = h(L,t) = 1$.

The first approach to this problem (Pedley, 1992) was based on lubrication theory, assuming negligible fluid inertia, steady flow and small wall slope: a one-dimensional model for low Reynolds number flow, but rationally derivable from the full equations of motion. The main innovation of that paper was its inclusion of the fact that the longitudinal tension in the membrane falls with downstream distance as a consequence of the viscous shear stress exerted by the fluid. However, the results were not qualitatively very different between the constant and variable tension cases, except when T fell close to zero. The main conclusion was that the steady problem has a solution, for all values of q and p_e, as long as T remains positive everywhere. For given positive values of longitudinal tension T_D and transmural pressure $p_e - p_D$ at the downstream end of the membrane (see Figure 6), the membrane is collapsed everywhere ($h < 1$ for all $0 < x < L$) for sufficiently small flow rate q, but exhibits a bulge outwards at its upstream end when q exceeds a critical value q_b. In these respects, the conclusions are the same as from the high Reynolds number one-dimensional model discussed above.

Even for low Reynolds number flow, the lubrication theory analysis was not uniformly valid because the wall slope became large at the downstream end in cases for which T_D was small. The next stage was therefore a numerical solution of the Stokes equations, coupled to the membrane equations. This was performed iteratively by Lowe and Pedley (1995), who used the finite element method to solve for the flow with the membrane position assumed given, calculated the pressure and shear stress exerted on the membrane, and then updated the membrane position by requiring that the membrane equilibrium equations be satisfied, and so on. This procedure led to predictions of membrane shape, for given values of q, T_D and $p_e - p_D$, which agreed remarkably well with the lubrication theory results even when the wall slope was quite large, but failed to give a solution for sufficiently small (but positive) values of membrane tension. We attribute this failure at small T_D to a poor iteration scheme for very compliant boundaries.

We now formulate the general problem for unsteady flow, although the next computation to be described will be for steady flow at non-zero Reynolds number (Luo and Pedley, 1995). The full governing equations and boundary conditions for the unsteady problem, in dimensionless form, are as follows, where velocities

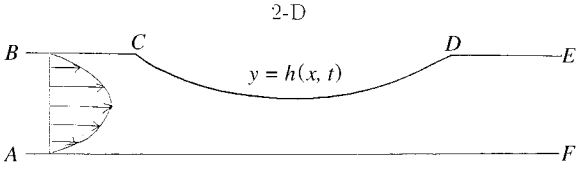

Figure 6. Sketch of the two-dimensional model problem.

are made non-dimensional with $u_0 = q/h_0$, time with h_0/U_0, stresses with ρU_0^2 (ρ is fluid density), and wall tension with $\rho U_0^2 h_0$; the Reynolds number is $Re = \rho U_0 h_0/\mu$ (μ is fluid viscosity) and the summation convention is used over suffixes $i, j = 1, 2$.

$$\text{Navier-Stokes} \qquad u_{i,t} + u_j u_{i,j} = -p_{,i} + Re^{-1} u_{i,jj}, \tag{10a}$$

$$\text{Conservation of mass} \quad u_{i,i} = 0. \tag{10b}$$

Boundary conditions (refer to Figure 6): on AB ($x = -L_\text{u}$),

$$u_1 = 6y(1-y), \qquad u_2 = 0; \tag{11a}$$

on EF ($x = L + L_\text{d}$),

$$-p + Re^{-1} u_{1,1} = 0, \qquad u_2 = 0; \tag{11b}$$

on BC, DE, AF ($y = 1$ for $x < 0$ or $x > L$; $y = 0$ for all x),

$$u_1 = u_2 = 0; \tag{11c}$$

on CD ($y = h(x,t), 0 \le x \le L$)

$$u_1 = u_2 = 0 \qquad \text{(steady)}, \tag{12a}$$

$$u_i = \text{velocity of membrane} \qquad \text{(unsteady)}, \tag{12b}$$

$$p_\text{e} - \sigma_\text{n} = T h_{xx} (1 + h_x^2)^{-3/2}, \tag{12c}$$

$$-\sigma_t = \partial T/\partial s. \tag{12d}$$

In the membrane equations (12c,d), σ_n and σ_t are the normal and tangential components of the stress exerted by the fluid on the membrane and s is the distance measured along the membrane. There should, in addition, be an equation relating the tension of each element of the membrane to its extension, but in this work we have assumed that T is independent of time, t, which is equivalent to assuming that the tension is sufficiently large for length variations to cause negligible changes in T. That suggests that the tension is also sufficiently large for the longitudinal variation to be negligible, so from henceforth we ignore condition (12d) and take T in (12c) to be a constant. The computations have confirmed that the overall length changes are no more than $\pm$ 4%, even during the most vigorous oscillations found (Luo and Pedley, 1996).

Although the non-dimensionalization described above is the most convenient for numerical solution, it is not convenient for the presentation of results because U_0 appears in the scalings for p_e and T. In presenting the results, therefore, we take

$$T = T_0/\beta Re^2, \qquad p_\text{e} = p_{e0}/\gamma Re^2, \tag{13}$$

where T_0 and p_{e0} are reference values, and increasing β or γ alone is equivalent to decreasing T or p_e at fixed Reynolds number Re.

Steady flow at finite Re was computed independently by Luo and Pedley (1995) and by Rast (1994), who both used the finite element method for the fluid flow, but used quite different techniques for coupling it to the membrane displacement. Luo and Pedley (1995) used the commercial flow solver FIDAP and iterated for the wall position in the manner described above in the context of Stokes flow. Rast (1994), on the other hand, used a finite element mesh which was coupled automatically to the membrane displacement by the method of spines (see Ruschak, 1980), and the membrane equation (12c) was discretized and solved simultaneously with the flow equations using Newton's method. The authors of both papers reported extensive accuracy tests, such as the effect of mesh refinement and adjustment of the location of the downstream boundary (i.e., the value of L_d), not only on membrane shape but also on the wall vorticity distribution, always one of the most sensitive tests of a CFD code. The best tests of all were agreement (a) between the results of the two computations and (b) with those of Lowe and Pedley (1995) at low Re (see Lowe *et al.*, 1996).

Both approaches to the steady problem, like Lowe and Pedley (1995), failed to find a convergent solution for sufficiently small, but positive, values of T (or sufficiently large β: (13)). Luo and Pedley (1995) discussed whether the breakdown was associated with the corner singularity at the upstream end of the membrane

(point C on Figure 6) when the membrane began to bulge out there. (Note the appendix to Lowe and Pedley (1995), in which Moffatt's (1964) corner solution is extended to the case where one of the walls is a membrane under tension.) However, Rast (1994) and more recent computations of our own (Luo and Pedley, 1996) have found converged solutions with upstream bulging; breakdown occurs at a much lower tension (for given Re) than bulging. We have concluded that such problems are extremely ill-conditioned when the boundaries are highly compliant (cf. free-surface flow (Ruschak, 1980)).

Steady Flow Results

Just the main features of the results are presented here; more details can be found in the original papers. One general finding is that qualitatively similar behaviour is obtained when Re is increased at fixed tension (β) as when tension is decreased (β increased) at fixed Re. In what follows we fix Re at the value 300 and vary β. Other dimensionless parameters (chosen for comparison with previous papers) are taken to be: $L = 5, L_u = 5, L_d = 30, T_0 = 1.61 \times 10^7,\ p_{e0} = 9.3 \times 10^4$ and $\gamma = 1$.

The membrane displacement for various values of β is plotted in Figure 7. At small β (large T) the membrane is stretched tight and is not deformed. As β is increased, the deformation increases, the minimum channel width $h_{\min}$ occurring close to the mid-point of the membrane. As the constriction becomes more severe, it tends to move downstream and a point of inflection appears in the upstream half. When β increases above about 30 two, possibly independent, phenomena are seen: the upstream part of the membrane begins to bulge out and the constriction, while continuing to move downstream, ceases to become more severe. In fact, $h_{\min}$ increases somewhat as β increases. The membrane slope becomes very large.

Both the above phenomena are also seen in the corresponding high-Reynolds-number one-dimensional model, which is exactly that of Jensen and Pedley (1989) described above ((1), (6), and (7)) but with h for A and $\tilde{P}(A) \equiv 0$. Indeed, the shape of the graph of $h_{\min}$ against β predicted by that model is very similar to that given by the full computation, as shown in Figure 8; the value of β at which bulging is first predicted is particularly close. The same is true at all Reynolds numbers from 50 to 500 (Luo and Pedley, 1995) though, as Re is decreased, $h_{\min}$ also falls, and occurs at larger β (smaller T). The one-dimensional model appears to be better than it deserves to be, at least in steady flow.

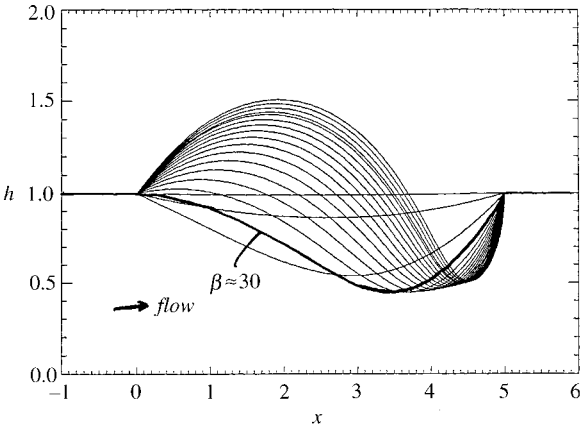

Figure 7. Predictions of steady membrane shape at Re = 300 and various values of tension parameter $\beta(\propto 1/T)$, from Luo and Pedley, 1996).

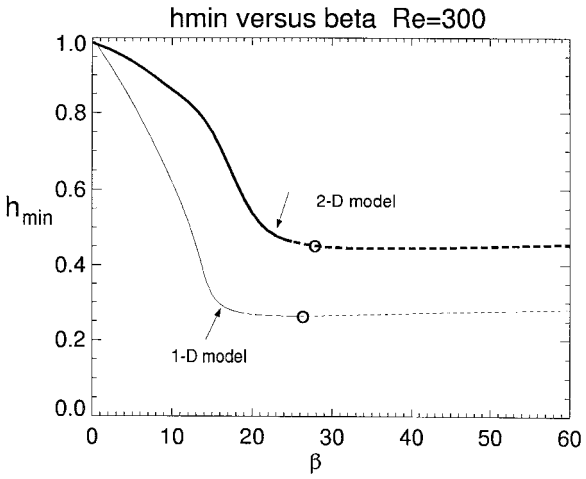

Figure 8. Predictions of minimum channel width during steady flow, plotted against β for fixed Re(= 300). Bold solid and broken curves, from the two-dimensional computations; fine solid and broken curves, from the one-dimensional model. The broken curves represent steady states that are subsequently found to be unstable. Circles mark the value of β at which upstream bulging first appears.

Unsteady Results

Extension of the above studies to time-dependent flow and membrane displacement required extensive development of the computational scheme.

The fully coupled finite element method of Rast (1994) was extended to deal with time dependence. The mesh was taken to be time-dependent, but based on fixed spines; Newton's method was used to obtain convergence at each time step. Details are given in Luo and Pedley (1996). The main difficulty concerned the kinematic boundary condition (12b), because it is necessary to track boundary points as they move, and that is not possible in the absence of a description of membrane elasticity. The boundary condition was eventually based on the assumption that elements of the membrane always move in a normal direction; this is not strictly true, but is reasonable. To check the importance of this boundary condition, we compared the results with those obtained with the even simpler assumption that boundary points move only in the y-direction. This is clearly less satisfactory (e.g., near the downstream end of the membrane) but fortunately there was not much difference in the results.

The unsteady code was used to investigate the stability of the steady solutions already computed (Luo and Pedley, 1996). The procedure was to start with a steady solution at a particular value of β, then increase the value of β by a small amount and start the computation; the initial condition was therefore a small displacement from the steady solution at the new value of β. For values of β less than a critical value β_c ($\approx$ 27.5 for Re = 300), the perturbation dies away, revealing the steady solution to be stable. For $\beta > \beta_c$, the perturbation grew and finite-amplitude oscillations ensued, showing that there had been a Hopf bifurcation. Examples of the behaviour are given in Figure 9, which shows the wall displacement h as a function of

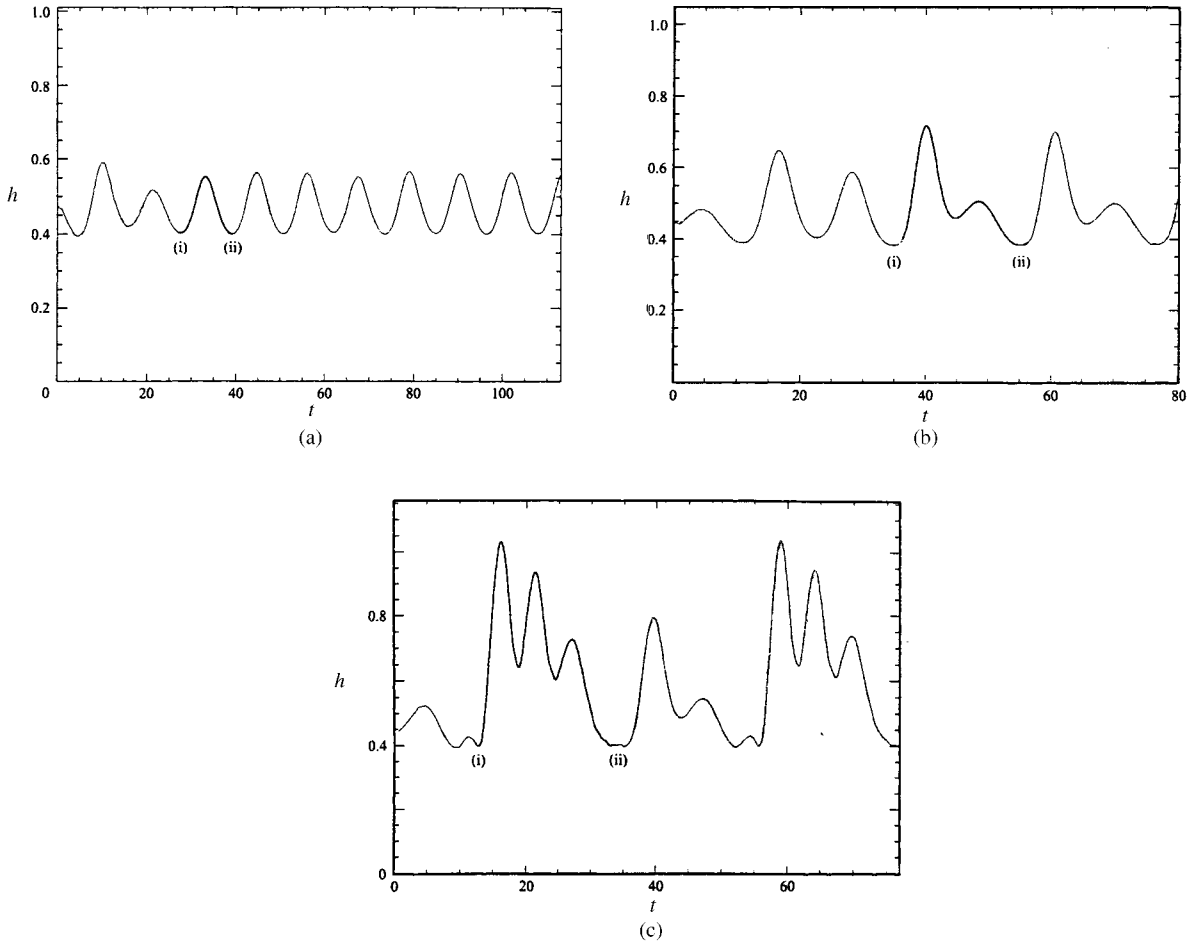

Figure 9. Membrane displacement h at fixed x = 3.5 as a function of time during self-excited oscillations. Re = 300; (a) β = 30.0, (b) β = 32.5, (c) β = 35.0.

time at a fixed value of x (x = 3.5, close to the site of greatest constriction in the steady solution) and for three values of β. For β = 30.0, Figure 9(a) shows an approximately sinusoidal oscillation, as is to be expected for a slightly supercritical value of β, with period 11.7 time units. However, for β = 32.5, Figure 9(b) shows a few cycles of adjustment, followed by a (nearly) periodic oscillation, of period 21–25, in which large maxima and minima alternate with small ones. It seems clear that the system has gone through a period-doubling bifurcation. Finally, Figure 9(c) shows the wall motion for β = 35.0; the wave-form is again more complex, indicating that at least one further bifurcation has occurred. We conclude that even this simple, two-dimensional, constant-tension model is an interesting dynamical system which may well incorporate some of the complexities of real collapsible tube flow.

Effect of Wall Inertia

Real membranes have mass, so it is important to see whether wall inertia has a significant effect on the computed oscillations. Wall inertia can be included (approximately) by adding a term $-mh_{tt}$ to the right-hand side of (12c), where

$$m = \rho_w w/\rho h_0 \tag{14}$$

and ρ_w, w are the density and thickness of the membrane. Estimates for a thin rubber membrane suggest that m = 0.01 is a reasonable value when the flowing fluid is water and m = 0.1 or greater when it is air. The computations and results are described in detail by Luo and Pedley (1997). In brief, putting m = 0.01 makes essentially no difference to the results reported above, but m = 0.1 has a considerable effect. Examples are shown in Figure 10. At β = 30 (Figure 10a), the regular oscillations are set up as before, but are gradually swamped by a high-frequency flutter which eventually grows to such large amplitude that the code breaks down. Even at β = 25 (Figure 10b), a previously stable state, high frequency flutter develops and grows large. These findings are consistent with those of experimentalists who have used air as well as water as the fluid flowing in a collapsible tube (e.g., Sakurai and Ohba (1986) compared with Ohba *et al.* (1984)).

Streamlines and Energy Dissipation

We revert now to the case of no wall inertia, in an attempt to understand the mechanism of the instability and oscillations. In Figure 11 we show the streamlines of the flow at various times during the oscillation cycle in just one case, that of Re = 300, β = 32.5 (Figure 9(b)). The important point to note is that the flow separation downstream of the narrowest point does not occur always at or near that point, as it would if the flow were quasi-steady. Moreover, waves are seen to be generated and to propagate downstream in the rigid channel downstream of the oscillatory membrane. These are clearly the same as the vorticity waves observed and analysed by Pedley and Stephanoff (1985); not only do they look the same, but the wavelength $\lambda \approx 3.6$ of the nearly sinusoidal oscillations of period ≈ 11.5 at β = 30 is comparable in magnitude with

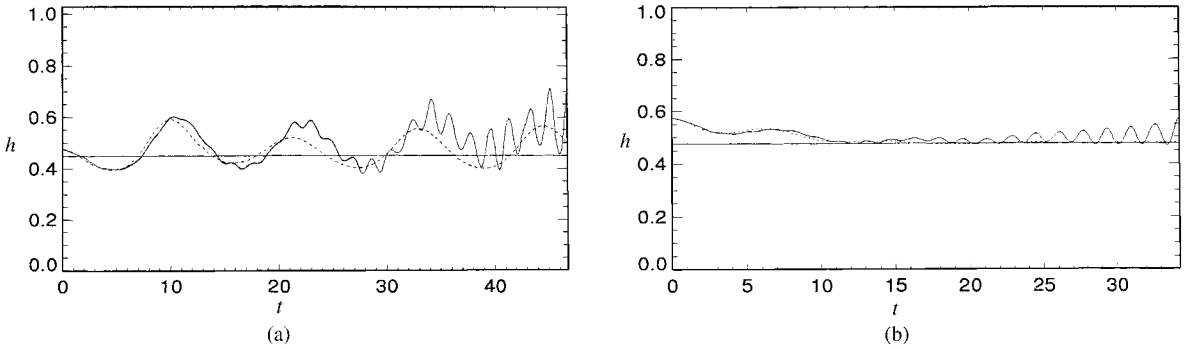

Figure 10. Membrane displacement h at x = 3.5 as a function of time t in the presence of wall inertia. Solid curves, m = 0.1; dotted curves, m = 0. Re = 300; (a) β = 30.0, (b) β = 25.0.

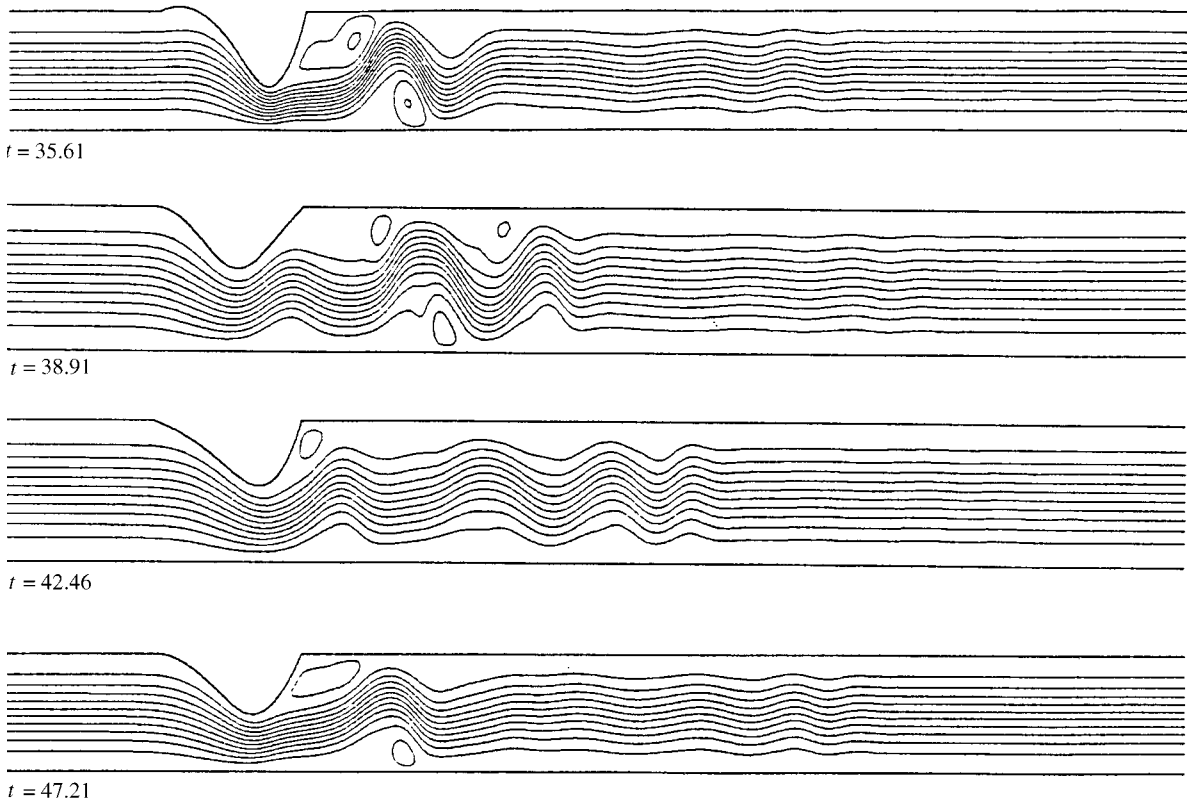

Figure 11. Streamline plots at various times during self-excited oscillations for Re = 300, β = 32.5.

those measured by Pedley and Stephanoff. Their run 5 with Re = 487 and the inverse of the dimensionless oscillation period, St, = 0.77 had wavelength $\approx$ 2.6; that was the shortest wavelength observed by those authors, corresponding to the highest value of St—theory suggests that $\lambda \propto St^{-1/3}$. (Note that what we call vorticity waves, because they are formed by the time-dependent, inviscid distortion of an oncoming flow with a non-zero vorticity gradient (cf. Rossby waves), are also an example of large-amplitude, inviscid Tollmien–Schlichting waves.) The streamline plots make it look as if the coupling between the vorticity waves and the flow separation process is somehow important for the latter, and hence for the separated flow energy loss that, according to the one-dimensional model, is a crucial feature in the system.

However, if we compute the rate of energy dissipation per unit volume, $\Phi = \mu u_{i,j}(u_{i,j} + u_{j,i})$, we are led in a different direction. Figure 12 shows contours of Φ for the same case and at the same times as the streamline patterns in Figure 11. The remarkable feature is that, at almost all times, the highest rates of energy dissipation occur in viscous boundary layers, on the membrane and on the opposite wall *upstream* of the point of greatest constriction, not downstream as postulated by Cancelli and Pedley (1985) and used in the subsequent one-dimensional models. There are occasional pockets of high dissipation, at the edges of the primary separated eddy and associated with the vorticity waves, but most of the dissipation is upstream. The volume integral of Φ over four equal segments of tube ($0 < x < 4,\ 4 < x < 8,\ 8 < x < 12,\ 12 < x < 16$) shows that the upstream segment contains the most dissipation all the time (Figure 13). The same is true for β = 30 (*a fortiori*), and for β = 35 except for a brief phase when the second segment, associated with the first separated eddy, has the most dissipation (see the corrigendum to Luo and Pedley (1996)).

A good physical explanation for the above findings still eludes us. Part of the difficulty is that the full time-dependent computations require very large computer resources, so we cannot examine parameter space in any detail. Instead, what we would like to do is to use the information obtained so far, especially that concerning energy dissipation, to develop a new one-dimensional model that is more soundly based than its predecessors.

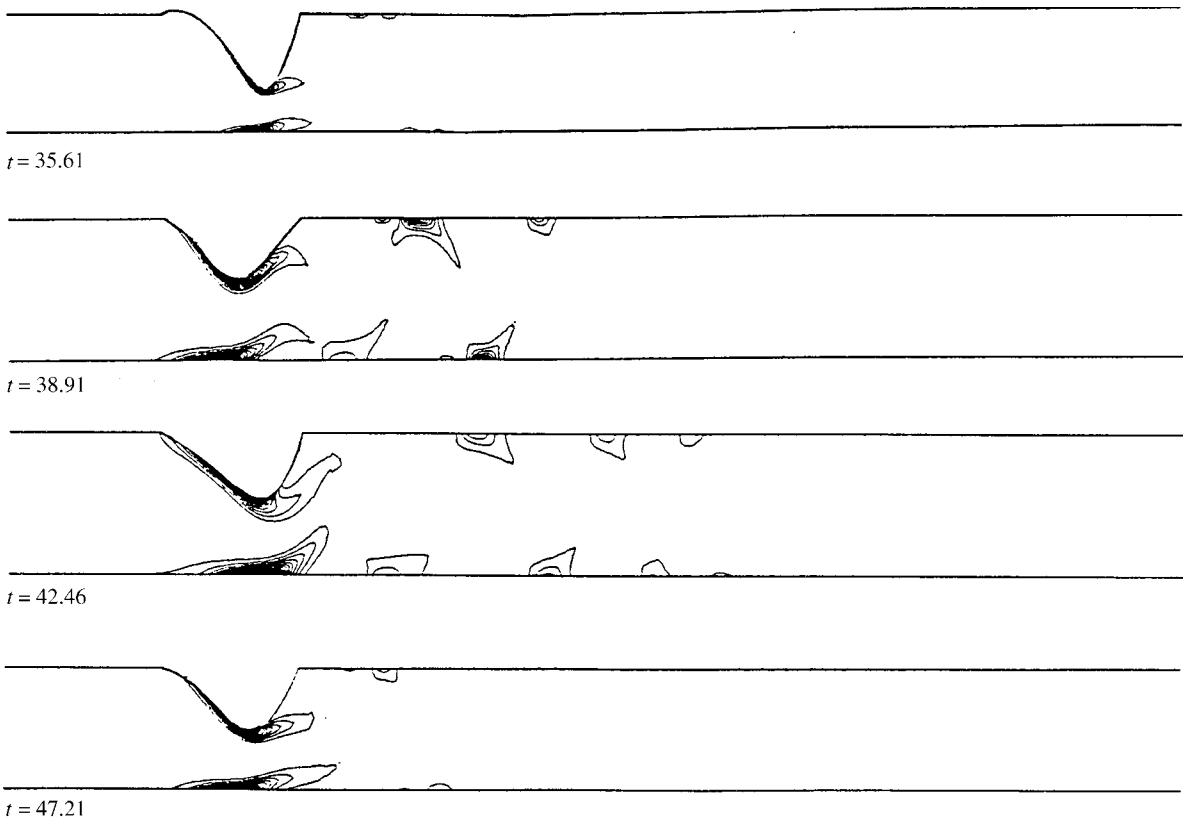

Figure 12. Contours of energy dissipation rate for the same parameters and times as the streamlines of Figure 11.

Towards a New One-Dimensional Model

The principal weakness of the old one-dimensional model, described in Section 2, is its treatment of loss terms in the longitudinal momentum equation. According to (7), energy dissipation is neglected upstream of the point of flow separation, and downstream of it is modelled very crudely. The separated flow energy loss is taken to be proportional to $-\partial\overline{u}^2/\partial x$, where $\overline{u}$ is the dimensionless longitudinal velocity, averaged across the channel. Amongst other things, that means that the dissipation comes to an end when the flow enters the downstream rigid channel, in which the pressure drop is taken to be given by a known non-linear resistance and linear inertance (Cancelli and Pedley, 1985). The full numerical solution shows that the primary separated eddy usually extends well into the rigid channel (see Figure 11) where, at least in unsteady flow, there are vorticity waves. Ideally, the new model will incorporate: calculation of the effects

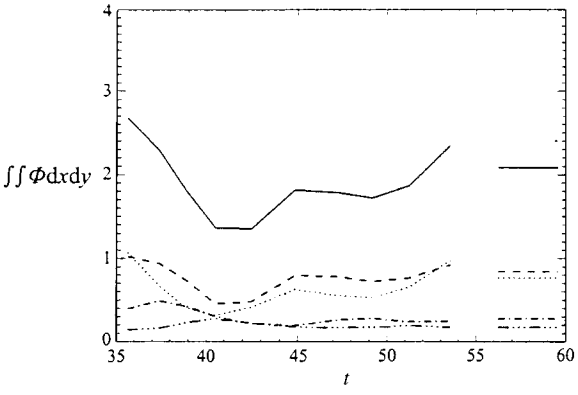

Figure 13. Total energy dissipation for four different segments of channel, plotted against time (Re = 300, β = 32.5); – – –, $0 < x < 4$; · · · · · ·, $4 < x < 8$; – · – · –, $8 < x < 12$; – · · · – · · · –, $12 < x < 16$; ——, total dissipation for $0 < x < 16$. Straight lines at the right give the dissipation in the corresponding steady flow. (From corrigendum to Luo and Pedley, 1996).

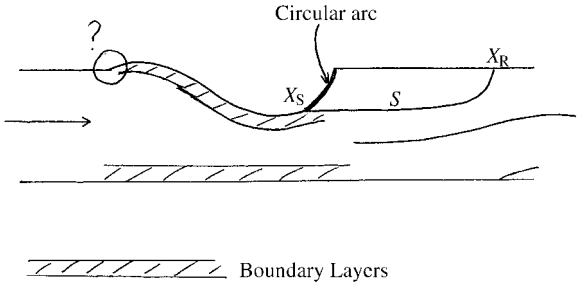

Figure 14. Sketch of the features that need to be incorporated in a new one-dimensional model.

of strong viscous boundary layers upstream of the point of flow separation, X_S (see Figure 14); prediction of that separation point and the reattachment point X_R, as functions of time; calculation of the contribution of the separated eddy S to the momentum equation; sufficient understanding of the coupling between vorticity wave generation and flow separation.

Some understanding of the separated eddy has been acquired by Ikeda and Matsuzaki (1997). They performed an experiment similar to that of Pedley and Stephanoff (1985), in which steady flow in a plane channel passed a known indentation which was either fixed or oscillating in a prescribed way with small amplitude. They tried to pinpoint X_S and X_R using flow visualisation, and they measured the pressure distribution along the plane wall ($y = 0$) as a function of position and time. They found that the measured pressures agreed well with those predicted from a model in which the separated eddy S was given a known shape, similar to that sketched in Figure 14: almost parallel-sided for most of its length, before a rapid termination at X_R. The flow was taken to be unidirectional in the core of the channel, with zero velocity in the eddy. The weakness of their model, from a predictive point of view, is that the positions of X_S and X_R have to be taken from experiment; moreover, they were taken to be unchanged from their steady values during the small-amplitude oscillations. (Ikeda and Matsuzaki recognized the weakness, and proposed a method of predicting X_S, at least in steady flow: see below.) The Ikeda and Matsuzaki model gives us some help in proposing a new model.

The equation of conservation of mass and the membrane equation will be the same as in previous models:

$$h_t + (\bar{u}h)_x = 0, \tag{15}$$

$$p_e - p = Th_{xx}(1 + h_x^2)^{-3/2}, \tag{16}$$

where the same non-dimensionalisation has been used as for the full two-dimensional equations and the viscous component of the normal stress (12c) has been neglected (it is in any case zero when the membrane is at rest). The x-momentum equation, integrated across the channel width, gives

$$\bar{u}_t + \bar{u}\bar{u}_x + \frac{1}{h}\frac{\partial}{\partial x}\left[\int_0^h u'^2\, dy\right] = -p_x + \frac{Re^{-1}}{h}[u'_y]_0^h, \tag{17}$$

where the longitudinal velocity $u(x, y, t) = \bar{u}(x, t) + u'(x, y, t)$, the pressure is assumed to be uniform across the channel, and longitudinal viscous diffusion has been neglected. The one-dimensional model would be complete if we had a rational way of linking the third and fifth terms in (17) to $\bar{u}, h$ and p, everywhere in the channel.

The procedure suggested by Ikeda and Matsuzaki (1977) for predicting the separation point X_s, in steady flow on a prescribed indentation, is to use the Karman–Pohlhausen approximation in which the velocity profile is replaced by a quartic polynomial in a suitably scaled transverse co-ordinate. Extending the idea to the time-dependent case in which the indentation is not prescribed, this means writing

$$\frac{u}{\bar{u}} = a\eta^4 + b\eta^3 + c\eta^2 + d\eta, \tag{18}$$

where $\eta = y/h$ and a, b, c, d are functions of x and t. The no-slip condition $u(x, 0, t) = 0$ is identically satisfied. The four functions a, b, c, d can be determined in terms of $\bar{u}, h$ and p and their derivatives from four equations representing: the no-slip condition on $y = h$ (which can be taken to be $u = 0$ if we assume the wall motion to be entirely in the y-direction): the definition of $\bar{u} = (1/h)\int_0^h u\, dy$; and the differential

x-momentum equation evaluated at $y = 0$ and $y = h$. Then substituting (18) into (17) gives the third partial differential equation linking $\overline{u}, h$, and p, to go with (15) and (16).

It might seem that this procedure could be used over most of the length of the membrane, marching forward from upstream boundary conditions that $h = 0$ at $x = 0$, and that the upstream velocity profile is parabolic. However, that is not possible because we do not know the relationship between the values of p so computed, and that of p_e, which is known only relative to the zero pressure far downstream. It is essential, therefore, to find a way of linking the pressure field under the membrane to that in the downstream rigid segment; i.e., we need a model of the primary separated eddy and the vorticity waves.

In steady flow, the Ikeda–Matsuzaki model again gives a hint: if there is zero velocity in the separated eddy S and parallel flow outside it, then the pressure will be uniform, and equal to its value at X_S. The consequence is that, from X_S to $x = L$, the membrane will form part of a circular arc. It only remains to predict the location of X_S and X_R and to model the pressure drop - flow rate relation downstream of X_R. The traditional way of predicting X_S, in steady flow, is to say that it occurs where the wall shear rate $u_y|_{y=h}$ is zero, and that was done by Ikeda and Matsuzaki (1997). A more rational choice would be to take separation to occur where $dp/dx = 0$, but in any case we have no correspondingly simple way of choosing X_R. Nevertheless, we have applied this new model, for steady flow, by fixing the downstream transmural pressure $p_e - p_s$ to be equal to a value obtained from the full numerical computation for the same Re and T (i.e., β), and by testing the difference between zero wall shear and zero pressure gradient as a separation criterion. (In most of the cases shown in Figure 15 below, p_s was taken to be equal to the value of p at $x = L$ in the full computation; in just one case it was taken equal to the minimum computed value of p.) An alternative model that we have also applied (for steady flow) is to continue to use the Karman–Pohlhausen approximation all the way to $x = L$.

Predictions of $h(x)$ and $p(x)$ according to the three new models are shown for one set of parameters ($\beta = 60, Re = 300$) in Figure 15 and compared with the full numerical solution. The new models agree pretty well with each other, but poorly with the corresponding two-dimensional calculation. The full solution shows a much stronger collapse of the downstream part of the membrane and a bigger bulge upstream, where the internal pressure is much greater. The full solution clearly involves much greater energy loss than the new approximations, and this must be due to the fact that the quartic velocity profile (18) cannot adequately represent the developing boundary layers and the separation process. That this is indeed so can be seen from the velocity profiles plotted in Figure 16, where it also becomes apparent (a) that the profile (18) is necessarily symmetric, while the real one is highly asymmetric, especially after flow separation, and (b) that the upstream bulge involves a distortion of the profile near the membrane which must be associated with some distortion further upstream ($x < 0$), precluded by the Karman–Pohlhausen method.

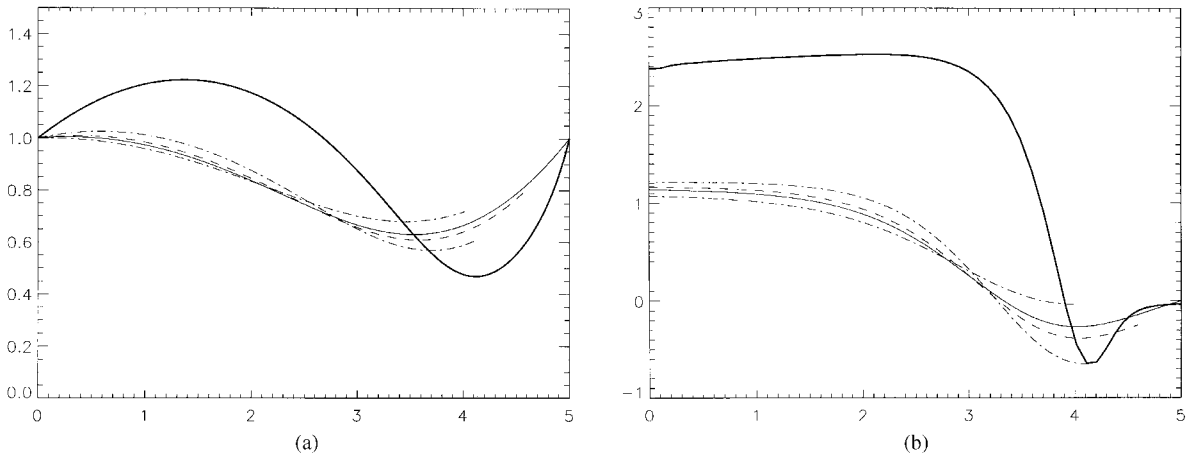

Figure 15. Results of the new models for steady flow, compared with the full computations ($Re = 300$, $\beta = 60$). (a) Membrane displacement $h(x)$; (b) pressure $p(x)$. Bold solid curves: full two-dimensional computations. Fine solid curves: new model used for all x; dashed curves: new model with a circular arc downstream of the separation point, defined by vanishing of wall shear rate; dash-dot curves: new model, with a circular arc downstream of the point of minimum pressure, and with transmural pressure taken to be the same as in the full model at either the downstream end or the minimum pressure point.

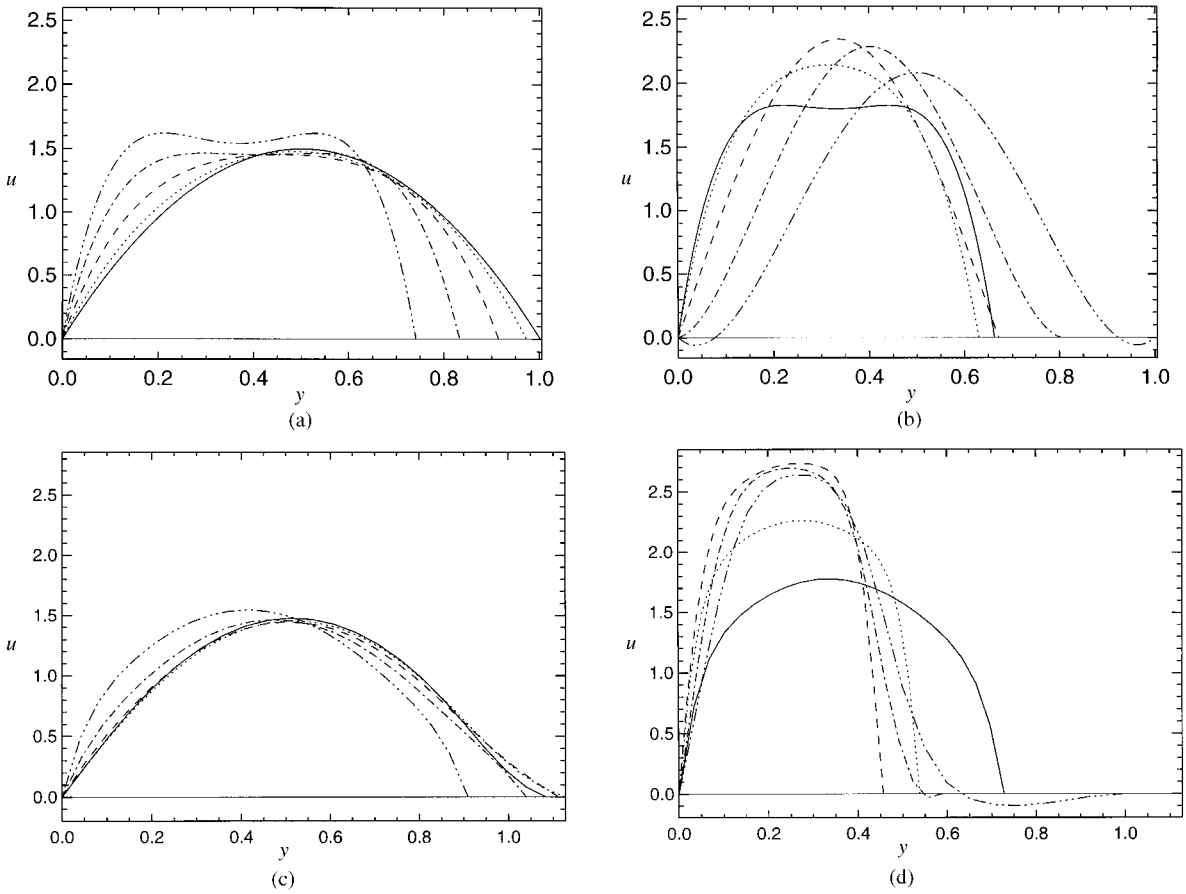

Figure 16. Velocity profiles at various values of x in steady flow, (a) and (b) according to the new model (using the Karman-Pohlhausen profiles all the way to $x = L$); (c) and (d) from the full computations. —— x/L = 0.1 (a) and (c), = 0.6 (b) and (d); · · · · ·, x/L = 0.2 (a) and (c), = 0.7 (b) and (d); – – –, x/L = 0.3 (a) and (c), = 0.8 (b) and (d); – · – · –, x/L = 0.4 (a) and (c), = 0.9 (b) and (d); – · · · – · · ·, x/L = 0.5 (a) and (c), = 1.0 (b) and (d)

We are currently working to improve the new one-dimensional model, using more modern boundary layer methods, both for steady flow and, more importantly, for unsteady flow. In the latter endeavour, a sensible way to match time-dependent flow separation to vorticity wave generation will be our primary goal.

Acknowledgements

T.J.P owes a profound debt of gratitude to Sir James Lighthill, for starting him off on the very fruitful path described in this paper and for all his support in many other ways over the years. We both wish to acknowledge the invaluable work of TJP's past and present collaborators in this area: Chris Bertram, Bindi Brook, Claudio Cancelli, Matthias Heil, Oliver Jensen, Roger Kamm, Tim Lowe, Mark Rast, Kyra Stephanoff, as well as many helpful conversations with Marc Bonis, Bill Conrad, Steve Cowley, Chris Davies, Yuji Matsuzaki, Kim Parker, Ascher Shapiro, and probably many others.

References

Bertram, C.D. (1982) Two modes of instability in a thick-walled collapsible tube conveying a flow. *J. Biomech.* **15**, 223–224.
Bertram, C.D. (1986) Unstable equilibrium behaviour in collapsible tubes. *J. Biomech.* **19**, 61–69.
Bertram, C.D. and Pedley, T.J. (1982) A mathematical model of unsteady collapsible tube behaviour. *J. Biomech.* **15**, 39–50.

Bertram, C.D. and Pedley, T.J. (1983) Steady and unsteady separation in an approximately two-dimensional indented channel. *J. Fluid Mech.* **130**, 315–345.
Bertram, C.D., Raymond, C.J. and Pedley, T.J. (1990) Mapping of instabilities during flow through collapsed tubes of differing length. *J. Fluids and Structures* **4**, 125–154.
Bertram, C.D. Raymond, C.J. and Pedley T.J. (1991) Application of non-linear dynamics concepts to the analysis of self-excited oscillations of a collapsible tube conveying a flow. *J. Fluids and Structures* **5**, 391–426.
Brecher, G.A. (1952) Mechanism of venous flow under different degrees of aspiration. *Amer. J. Physiol.* **169**, 423–433.
Brower, R.W. and Scholten, C. (1975) Experimental evidence on the mechanism for the instability of flow in collapsible vessels. *Med. Biol. Engrg.* **13**, 839–844.
Cancelli, C. and Pedley, T.J. (1985) A separated flow model for collapsible tube oscillations. *J. Fluid Mech.* **157**, 375–404.
Conrad, W.A. (1969) Pressure-flow relationships in collapsible tubes. *IEEE Trans. Bio-Med. Engrg.* **BME-16**, 284–295.
Danaky, D.T. and Ronan, J.A. (1974) Cervical venous hums in patients on chronic hemodialysis. *New Engl. J. Med.* **291**, 237–239.
Flaherty, J.E., Keller, J.B. and Rubinow, S.I. (1972) Post-buckling behaviour of elastic tubes and rings with opposite sides in contact. *SIAM J. Appl. Math.* **23**, 446–455.
Heil, M. and Pedley, T.J. (1996) Large post-buckling deformations of cylindrical shells conveying viscous flow. *J. Fluids and Structures* **10**, 565–599.
Ikeda, T. and Matsuzaki, Y. (1997) A one-dimensional unsteady separable and reattachable flow theory for collapsible tube flow analysis (submitted to *ASME J. Biomech. Engrg.*).
Jensen, O.E. (1990) Instabilities of flow in a collapsed tube. *J. Fluid Mech.*, **220**, 623–659.
Jensen, O.E. (1992) Chaotic oscillations in a simple collapsible-tube model. *ASME J. Biomech. Engrg.* **144**, 55–59.
Jensen, O.E. and Pedley, T.J. (1989) The existence of steady flow in a collapsed tube. *J. Fluid Mech.* **206**, 339–374.
Kamm, R.D. and Pedley, T.J. (1989) Flow in collapsible tubes: a brief review. *ASME J. Biomech Engrg.* **111**, 177–179.
Katz, A.I., Chen, Y. and Moreno, A.H. (1969) Flow through a collapsible tube. *Biophys. J.* **9**, 1261–1279.
Lighthill, J. (1975) *Mathematical Biofluiddynamics*, SIAM, Philadelphia, PA.
Lowe, T.W. and Pedley, T.J. (1995) Computation of Stokes flow in a channel with a collapsible segment. *J. Fluids and Structures* **9** 885–905.
Lowe, T.W., Luo, X.-Y. and Rast, M.P. (1996) A comparison of three solution methods for flow in a collapsible channel. (private communication).
Luo, X.Y. and Pedley, T.J. (1995) A numerical simulation of steady flow in a 2-D collapsible channel. *J. Fluids and Structures* **9**, 149–174.
Luo, X.-Y. and Pedley, T.J. (1996) A numerical simulation of unsteady flow in a 2-D collapsible channel. *J. Fluid Mech.*, **314**, 191–225 (corrigendum **324**, 408–409).
Luo, X.-Y. and Pedley, T.J. (1997) The effects of wall inertia on flow in a 2-D collapsible channel (submitted to *J. Fluid Mech.*).
Moffatt, H.K. (1964) Viscous and resistive eddies near a sharp corner. *J. Fluid Mech.* **18**, 1–18.
Ohba, K., Yoneyama, N., Shimanaka, Y. and Maeda, H. (1984) Self-excited oscillation of flow in collapsible tubes. *Tech. Rep. Kansai Univ.* **25**, 1–13.
Pedley, T.J. (1980) *The Fluid Mechanics of Large Blood Vessels*, Cambridge University Press, Cambridge.
Pedley, T.J. (1992) Longitudinal tension variation in collapsible channels: a new mechanism for the breakdown of steady flow. *ASME J. Biomech. Engrg.* **114**, 60–67.
Pedley, T.J., Brook, B.S. and Seymour, R.S. (1996) Blood pressure and flow rate in the giraffe jugular vein. *Philos. Trans. Roy. Soc. London. Ser. B* **351**, 855–866.
Pedley, T.J. and Stephanoff, K.D. (1985) Flow along a channel with a time-dependent indentation in one wall: the generation of vorticity waves. *J. Fluid Mech.* **160**, 337–367.
Rast, M.P. (1994) Simultaneous solution of the Navier–Stokes and elastic membrane equations by a finite-element method. *Internat. J. Numer. Methods. Fluids* **19**, 1115–1135.
Ruschak, K.J. (1980) A method for incorporating free boundaries with surface tension in finite element fluid-flow simulators. *Internat. J. Numer. Methods Engrg.* **15**, 639–648.
Sakurai, A. and Ohba, K. (1986) Self-excited oscillation of flow in collapsible tube, III. *Tech Rep. Kansai Univ.* **28**, 41–48.
Schoendorfer, D.W. and Shapiro, A.H. (1977) The collapsible tube as a prosthetic vocal source. *Proc. San Diego Biomed. Symp.* **16**, 349–356.
Shapiro, A.H. (1977a) Steady flow in collapsible tubes, *ASME J. Biomech. Engrg.* **99**, 126–147.
Shapiro, A.H. (1977b) Physiologic and medical aspects of flow in collapsible tubes. *Proc. 6th Canadian Congress on Applied Mechanics*, pp. 883–906.
Ur, A. and Gordon, M. (1970) Origin of Korotkoff sounds. *Amer. J. Physiol.* **218**, 524–529.